# A Versatile Multicomponent Assembly via β-cyclodextrin Host–Guest Chemistry on Graphene for Biomedical Applications

*Haiqing Dong, Yongyong Li,* Jinhai Yu, Yanyan Song, Xiaojun Cai, Jiaqiang Liu, Jiaming Zhang, Rodney C. Ewing, and Donglu Shi**

***A** multi-component nanosystem based on graphene and comprising individual cyclodextrins at its surface is assembled, creating hybrid structures enabling new and important functionalities: optical imaging, drug storage, and cell targeting for medical diagnosis and treatment. These nanohybrids are part of a universal system of interchangeable units, capable of mutilple functionalities. The surface components, made of individual β-cyclodextrin molecules, are the "hosts" for functional units, which may be used as imaging agents, for anti-cancer drug delivery, and as tumor-specific ligands. Specifically, individual β-cyclodextrin (β-CD), with a known capability to host various molecules, is considered a module unit that is assembled onto graphene nanosheet (GNS). The cyclodextrin-functionalized graphene nanosheet (GNS/β-CD) enables "host–guest" chemistry between the nanohybrid and functional "payloads". The structure, composition, and morphology of the graphene nanosheet hybrid have been investigated. The nanohybrid, GNS/β-CD, is highly dispersive in various physiological solutions, reflecting the high biostability of cyclodextrin. Regarding the host capability, the nanohybrid is fully capable of selectively accommodating various biological and functional agents in a controlled fashion, including the antivirus drug amantadine, fluorescent dye [5(6)-carboxyfluorescein], and Arg-Gly-Asp (RGD) peptide-targeting ligands assisted by an adamantine linker. The loading ratio of 5(6)-carboxyfluorescein is as high as 110% with a drug concentration of 0.45 mg $mL^{-1}$. The cyclic RGD-functionalized nanohybrid exhibits remarkable targeting for HeLa cells.*

Dr. H. Q. Dong, Dr. Y. Y. Li, J. H. Yu, Y. Y. Song, X. J. Cai, J. Q. Liu, Prof. D. Shi
The Institute for Biomedical Engineering and Nano Science
Tongji University School of Medicine
Shanghai 200092, P.R. China
E-mail: yongyong_li@tongji.edu.cn; shid@ucmail.uc.edu
Prof. D. Shi
School of Electronic and Computing Systems
University of Cincinnati
Cincinnati, OH 45221, USA
Dr. J. M. Zhang, Prof. R. C. Ewing
Department of Materials Science & Engineering
University of Michigan
Ann Arbor, Michigan 48109, USA

DOI: 10.1002/smll.201201003

## 1. Introduction

For biomedical applications, a nanocarrier is typically developed with a variety of functional groups for conjugation with biological molecules including DNA, RNA, antibodies, and other species that are needed in diagnosis and therapy. However, this current approach is often complicated, and the synthesis and processing remain a challenge due to structural and chemical incompatibilities among the nanocarriers, functional groups, and biological molecules. As an example, the integration of individual components can lead to by-products of aggregated chemical species.[1,2] The multifunctionalities required for medical diagnosis and treatment cannot be easily and reproducibly assembled into a compact nanosystem. These components include a biocompatible nanocarrier of a preferred geometry, on which the anti-tumor drug can

NANO MICRO small

be sufficiently loaded for controlled release at the lesion. A fluorescent dye having an emission, preferably in the near-infrared range, is needed for in vitro or in vivo imaging. For cancer cell targeting, the nanocarrier has to be functionalized with a tumor specific ligand. However, the assembly of these basic components is also complicated by drastically different intrinsic behaviors of the nanocarriers. For medical applications, lacking of consistency and reproducibility in these multifunctional carriers will present a major barrier to future clinical applications. Therefore, these nanocarriers must be developed with controlled overall sizes, component ratios, and biophysical properties. It is also particularly important for the carriers to exhibit controlled drug release and other therapeutic effects such as magnetic hyperthermia.

The current challenges in the development of multi-functional systems have been that the conventional nanocarriers are often limited by their intrinsic structural, physical, and chemical complexities. In this study, a versatile nanosystem with multifunctionalities was developed with graphene as universal platform, on which cyclodextrins (CDs) were anchored with multiple accommodating sites for various functional units.

Graphene is used to develop the nanocarrier system for medical imaging, drug delivery, and cell targeting. Graphene nanosheet (GNS), a single layer of carbon atoms in a two dimensional, close-packed, planar honeycomb structure, is a structurally well-defined system, which has been utilized for biomedical applications, such as biosensors,[3,4] drug delivery,[5–8] imaging etc.[4,9–11] The unique characteristics of GNS includes extraordinary electrochemical properties, non-covalent interaction with many aromatic pharmaceuticals, and a super-high surface area. In most of the biomedical applications, GNS has to be surface functionalized for its manipulation in biological solutions, as strong $\pi$–$\pi$ interactions between individual GNS easily result in irreversible agglomerates or even the formation of graphite.[12] Its oxide derivative, rich in carboxyl, hydroxyl and epoxy groups, enables GNS to be highly dispersible in pure water. However, the properties of the oxide formulation are often compromised by the partially destroyed planar structure in the oxidation process. Furthermore, it suffers from instability in biological solutions such as culture medium and serum, which is reported to be associated with the screening effect of the electrostatic charges and nonspecific binding of proteins. These complications and shortcomings have severely limited graphene applications in biomedical diagnosis and treatment.

Thus, we propose a new system that provides multiple functionalities while maintaining its high structural integrity and dispersity. PEG functionalization has been a very useful approach for modifying nano-graphene oxide with fragmentary $\pi$–$\pi$ structure.[13–15] Pluronic F127-,[16] chitosan-,[17] and dextran-[18] functionalized graphene oxide have also been recently reported. These methods have effectively improved the biological dispersity and biocompatibility of graphene. However, the graphene structure remains disordered in the carbon skeleton due to a random arrangement of oxygen functional groups, which may pose negative effects on its electrochemical properties,[19,20] as well as their drug loading capability.[21] On the other hand, drug release and cell internalization of the nanohybrid can be limited by the use of surface coated polymers. A PEG selective detachment mechanism was recently developed that could effectively release drugs in a tumor specific environment.[22]

In consideration of these GNS structural characteristics for biomedical requirements, a versatile nano-assembly is designed and developed in this study. The system is engineered on a nanoscaled GNS platform *via* host–guest chemistry between the hybrid and functional payloads. Cyclodextrin (CD), an oligosaccharide consisting of six, seven or eight glucose units ($\alpha$, $\beta$, or $\gamma$-CD, respectively), is utilized as the "host" molecule. This cone-shaped cavity of CDs can serve as hosts for a great variety of functional or biological "guest" molecules by taking advantage of its geometric compatibility and hydrophobic interactions between the CDs and the guest molecules.[23,24] As such, CDs have been widely used in biomedical applications, such as drug formulations, tissue engineering, and gene/drug delivery.[25]

In this design, as shown in **Scheme 1**, multiple CDs are anchored onto GNS in a "one pot" reduction process of nano-graphene oxide in the presence of ammonia, resulting in a GNS/CD nanohybrid. The GNS/CD nanohybrid, with relative integrated $\pi$–$\pi$ structure and biological dispersity, is capable of hosting multiple functional and biological guests. Each CD may be regarded as an individual module that enables the "host–guest" mechanism to accommodate various functional units for biomedical applications.

A wet-chemical strategy was adopted for the GNS/CDs nanohybrid preparation in this study. The experimental results indicate that the nanohybrid is highly stable in biological environment and fully capable of selectively accommodating various biological and functional agents, including antivirus drug amantadine, fluorescent dye (5(6)-carboxyfluorescein), and the Arg-Gly-Asp (RGD) peptide-targeting ligands assisted with an adamantine linker, which are critical to tumor diagnosis and therapy. The controlled release capability of the bio-agents can be regulated by adding competitive guest molecules via the reversibility of host–guest interaction.[26]

## 2. Results and Discussion

### 2.1. Preparation and Characterization of the GNS/β-CD Hybrid

Generally, the reduction of graphene oxide proceeds in the presence of weak alkaline condition.[27] Herein, $\beta$-CD, as a model host molecule, was assembled onto GNS within the process of graphene oxide (GO) reduction in the presence of ammonia aqueous solution, affording the graphene nanosheets (GNS/CD). The whole process avoids the utilization of toxic reduction agent, such as hydrazine or its derivates. In order to demonstrate the functionality of $\beta$-cyclodextrin in the process of reduction, a controlled experiment was carried out for GO reduction without ammonia, or $\beta$-CD, or both under otherwise identical conditions. The GO solution changed from brown to black in concomitance with the rapid precipitation of congeries occurring in the presence of only ammonia, which mainly ascribed to reduced oxygen containing groups resulting in the low dispersion capacity for GNS in aqueous phase. The X-ray photoelectron spectroscopy (XPS) results show a higher C/O

  

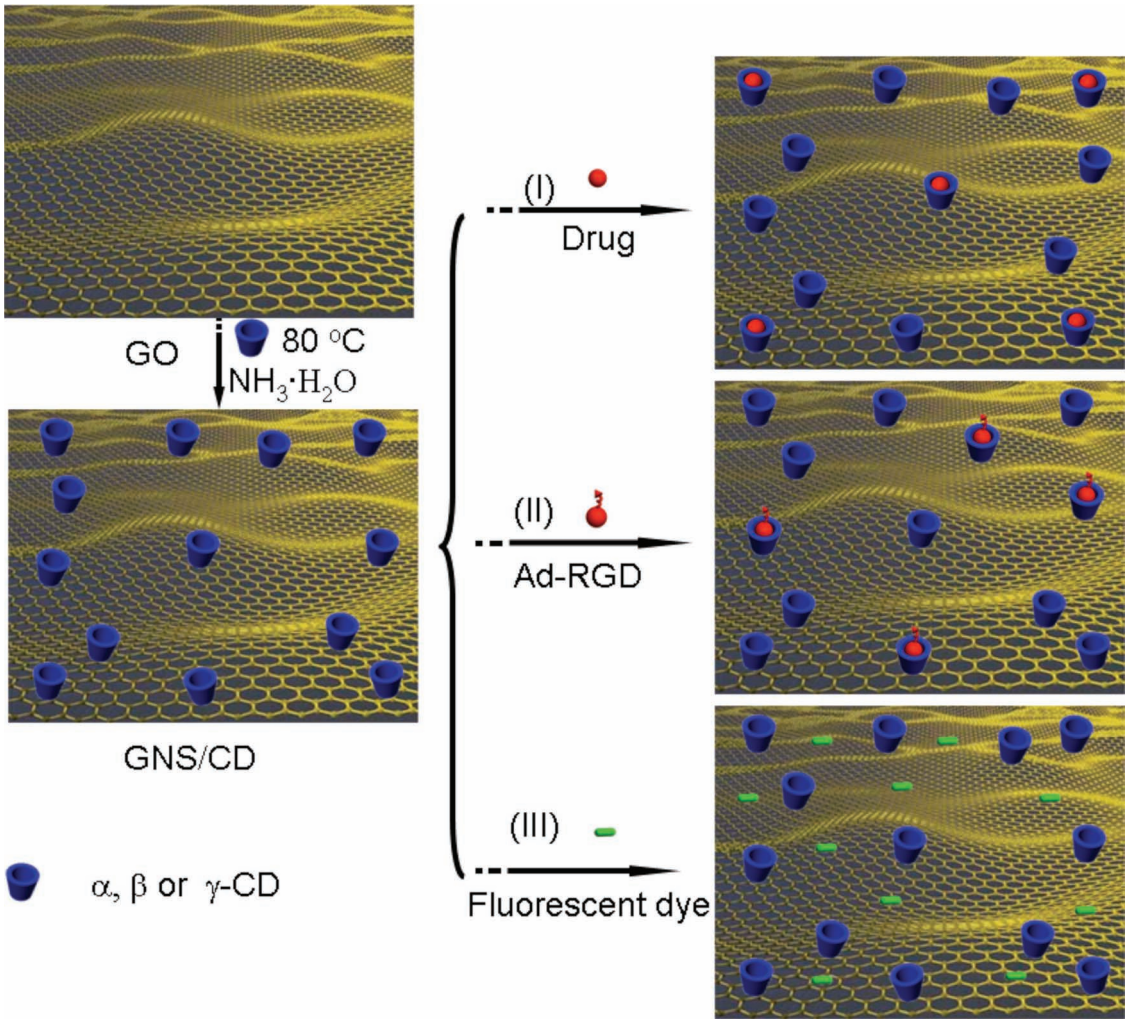


**Scheme 1.** Schematic illustration for GNS/CD formation and "host and guest" functionalization. GNS/CD nanohybrid, surface capped with large quantities of cavities (cyclodextrins), can be used to "host" various functional guests including antivirus drug amantadine, or RGD targeting ligands assisted by an adamantine linker.

molar ratio (2.6) for GNS than that for GO (2.2) (see Figure S1), indicating successful reduction. GNS obtained in ammonia aqueous solution with β-CD exhibits good dispersion in water for a prolonged time without sinking, suggesting the stabilizing role of β-CD. Zeta potential shows a strong correlation with the oxidation level, as indicated by the functional groups, such as COOH, mainly located at the edges of the graphene oxide sheets. Weak negative charges are developed in the solution due to COOH deprotonation. Zeta potentials of colloid GO and GNS/β-CD are –24 mV and –19 mV, respectively at the same concentration of 35 mg $L^{-1}$ with comparable size. These are clear evidences of reduction. In contrast, no obvious reduction was found in the controlled experiment with the absence of both β-CD and ammonia.

Raman spectroscopy was employed to characterize the structural changes during the chemical processes from graphite to GO and GNS. The typical features in the Raman spectra of flake graphite display a prominent G band at 1581 $cm^{-1}$ and an extremely weak D band at 1352 $cm^{-1}$, while GO and GNS/β-CD both show pronounced G band around 1594 $cm^{-1}$ and the D band at 1352 $cm^{-1}$ (**Figure 1**). The G band is usually

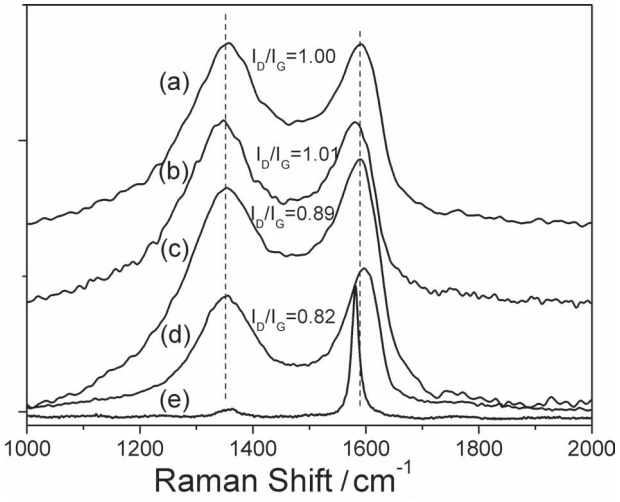


**Figure 1.** Raman spectra of GNS obtained from (a) GO with $NH_3 \cdot H_2O$; (b) GO with β-CD and $NH_3 \cdot H_2O$; (c) GO with β-CD; (d) GO only at the same reaction conditions of 80 °C; (e) flake graphite. Using Raman spectrometer (Renishaw inVia Reflex, UK) with argon ion laser emitting at 514.5 nm (20 mW).

small NANO MICRO

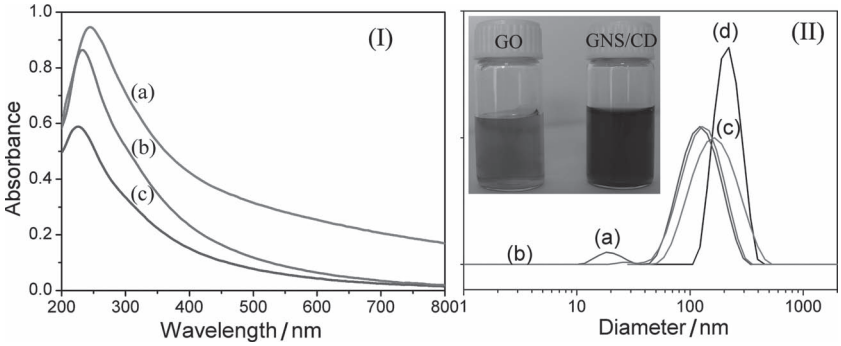


**Figure 2.** (I) UV-vis absorption spectra of GO dispersion (c) and after reduction with ammonia and β-cyclodextrin at 80 °C for 2 h (a) and 1 h (b), respectively. (II) Size of GO (a); GNS/β-CD (b) and GNS/β-CD stored at room temperature for one month (c) and three months (d). Inset shows the color change of 0.05 mg $mL^{-1}$ GO solution before and after reduction.

arisen from the $E_{2g}$ phonon of $sp^2$ atoms, and the D band is a breathing mode of k-point phonons of $A_{1g}$ symmetry. The intensity ratio ($I_D/I_G$) of D band to G band in graphitic materials has been used to determine the size of $sp^2$ domains.[28] The $I_D/I_G$ ratios for GO and GNS are respectively 0.82 and 1.0, obtained from GO with ammonia or β-CD and ammonia. The ratio increase, as reported by Ruoff, indicates the decrease in size of $sp^2$ domains,[29] resulting from the increased number of smaller nascent $sp^2$ domains during reduction process.[30] In contrast to GO reduction in the presence of only β-CD, the slightly increased $I_D/I_G$ ratio (0.89) also suggests a decrease in size of sp2 domains. However, the extent of decrease is not as high as in the presence of ammonia based on the comparison of the intensity ratio of characteristic D to G band in the Raman spectra (Figure 1). This indicates the involvement of CD in the reduction process.

UV-vis spectroscopy was used to monitor the reduction process of GO to GNS as a function of time. To this end, 1 mL of reactant dispersion was removed from the reaction vial every 1 h and their UV-vis spectrum was recorded. As shown in **Figure 2**I, the typical UV-vis absorption peak of GO dispersion appears at 230 nm, which is due to the $\pi$–$\pi^*$ transition of aromatic C=C bonds. After reduction in the presence of ammonia and β-CD, the maximum absorption peak gradually red-shifts to 256 nm and the absorption increases in the entire spectral region for prolonged reduction. It is likely that the oxygen-containing functional groups on GO have been removed in the presence of β-cyclodextrin under weak alkaline condition accompanied by the formation of new π-conjugation network of the graphene nanosheets upon deoxidation. The evidence of reduction is also demonstrated from the color change of the solution before and after reaction. The light brown of GO darkens after reduction (Figure 2II inset) with no obvious size change. By dynamic light scattering (DLS) monitoring, it is found that most of GO in aqueous solution is around 120 nm with a small population on the order of ~20 nm. After reduction in the presence of β-CD and ammonia for 2 h, the size is maintained at ~120 nm with no obvious change. Particularly, the as-prepared graphene dispersion show long-term stability in water, and no pronounced aggregation or precipitation is observed after more than one month of storage at room temperature, as determined by DLS monitoring shown in Figure 2II.

The removal of oxygen-containing functional groups on the GO surface through β-CD reduction is also confirmed by FTIR spectroscopy. The FTIR spectra of GO (**Figure 3**) show a strong and broad absorption peak at 3403 $cm^{-1}$ corresponding to the stretching vibration of O–H, and a peak at 1605 $cm^{-1}$ due to O–H bending vibration. A diagnostic signal at 1730 $cm^{-1}$ for C=O stretching vibration of COOH is observed. Meanwhile, the absorption peaks of the epoxide groups and skeletal ring vibrations are situated at 1060 $cm^{-1}$ and 1617 $cm^{-1}$, respectively. For GNS/β-CD in Figure 3a, the signal of C=O at 1730 $cm^{-1}$ is absent, suggesting that GO has been reduced to graphene nanosheets. The new absorption peak at around 2918 $cm^{-1}$ is mainly attributed to the stretching vibration of C–H as well as the typical CD absorption fingerprint peaks in the range of 500~1100 $cm^{-1}$ (Figure 3c), confirming the attachment of CD on GNS.

$^1$HNMR data disclose the structural alterations of β-CD before and after reduction process, where the characteristic peaks of β-CD are assigned in the **Figure 4**. A decreased integrated area for hydroxyl groups (OH-2, OH-3, OH-6) of CDs in GNS/β-CD, in comparison with pure β-CD, is observed (Figure 4a,b). This suggests that the portion of primary and secondary hydroxyl groups of β-CD have been converted to other groups like aldedydes/carboxyl groups and ketones, respectively as reported.[27,31,32] Carboxyl groups are less likely, since aldedydes or ketones may further react with hydroxyl groups on graphene oxide resulting in formation of hemiacetal or acetal, which affords the GNS/β-CD formation. Two facts support this assumption: i) C=O stretching band is hardly be detected in the FTIR spectra of GNS/β-CD indicating the insignificant role of the involvement of carboxyl

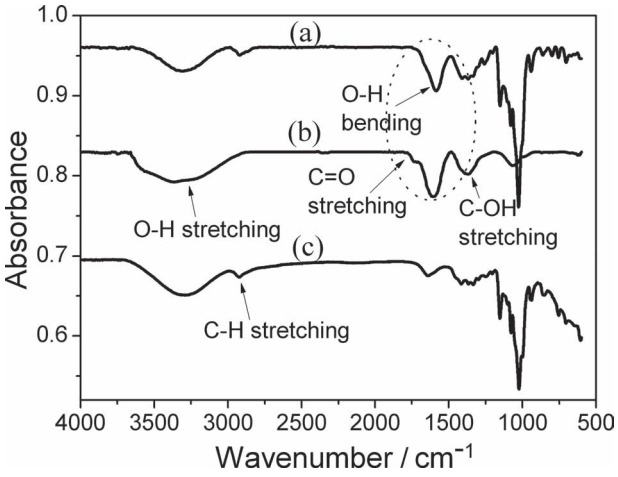


**Figure 3.** FTIR spectra of GNS/β-CD (a), GO (b), and β-CD (c) collected using a Tensor 27 FTIR spectrometer.

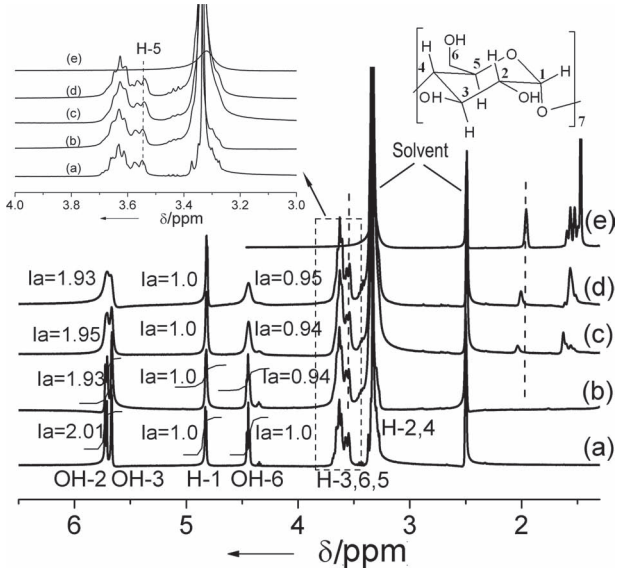


Figure 4. $^1$H NMR spectra of $\beta$-CD (a), freeze-dried GNS/$\beta$-CD (b), freeze-dried GNS/$\beta$-CD/Ad-$NH_2$ with increasing loading ratio of Ad-$NH_2$ [(c) 3.88 wt%, (d) 5.71 wt%] and Ad-$NH_2$ (e). (DMSO-*d6* as solvent, "Ia" denotes integrated area)

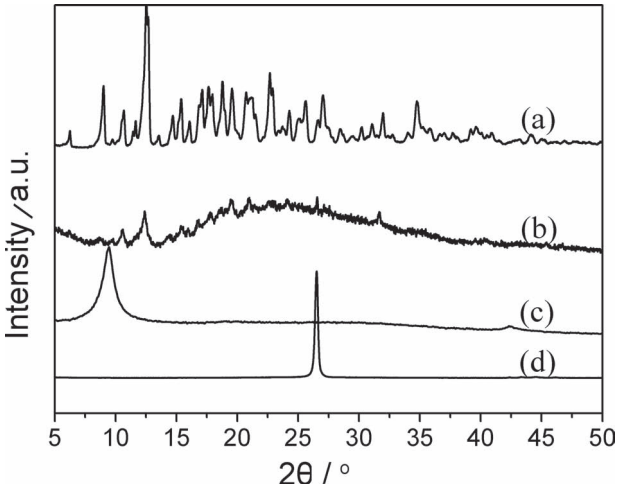


Figure 5. XRD patterns of $\beta$-CD (a), GNS/$\beta$-CD (b), GO (c), and graphite (d). CuK$\alpha$ (40 kV, 100 mA) as radiation source with a scanning rate of 4° min$^{-1}$ at 20 °C.

groups, and ii) GNS/$\beta$-CD exposed to acid environment experiences fast aggregation in few minutes. This behavior is associated with decomposition of GNS/$\beta$-CD by acid cleavable hemiacetal or acetal, leading to hydrophobic GNS precipitation. However, the exact products generated in this process are yet to be identified due to the complicated chemical environment in this unique composite system.

**Figure 5** shows the X-ray diffraction (XRD) patterns of $\beta$-CD, pristine graphite, GO, and GNS/$\beta$-CD. XRD pattern of GO (Figure 5c) shows a single sharp diffraction peak at $2\theta = 9.34°$ corresponding to an interlayer distance of 0.83 nm. This value is larger than the interlay spacing of pristine graphite, which is 0.34 nm at $2\theta$ = 26.5° (Figure 5d). This can be ascribed to the presence of oxygen-containing functional groups, as well as the water molecules held in these groups.[33] In contrast, the diffraction peak of GNS/$\beta$-CD hybrid (Figure 5b) does not show any residual at $2\theta$ = 9.34° after chemical reduction. At the same time, a strong broad peak is observed at approximately $2\theta$ = 23.3° with an interlayer distance of 0.34 nm. These results indicate the removal of the oxygen-containing functional groups and the reduction of GO. The XRD pattern of GNS/$\beta$-CD also shows the similar characteristics of $\beta$-CD (Figure 5a), indicating the presence of $\beta$-CD on the surface of GNS.

X-ray photoelectron spectroscopy (XPS) was completed in order to further confirm the removal of the oxygen-containing functional groups. C1s XPS results (**Figure 6**) show that four components are found to be associated with carbon atoms in the C 1s region. The peak located at 284.5 eV is attributed to the $sp^2$ carbon components, and C 1s of C–O, C=O, and O–C=O are observed at 286.6 ev, 287.8 eV and 288.9 eV, respectively. For the GNS/$\beta$-CD hybrid (Figure 6b), the peak intensities corresponding to C=O and O–C=O are much lower than that of GO, indicating effective reduction of GO. The C–O peak intensity increases mainly due to the presence of $\beta$-CD, which is confirmed by the lower intensity

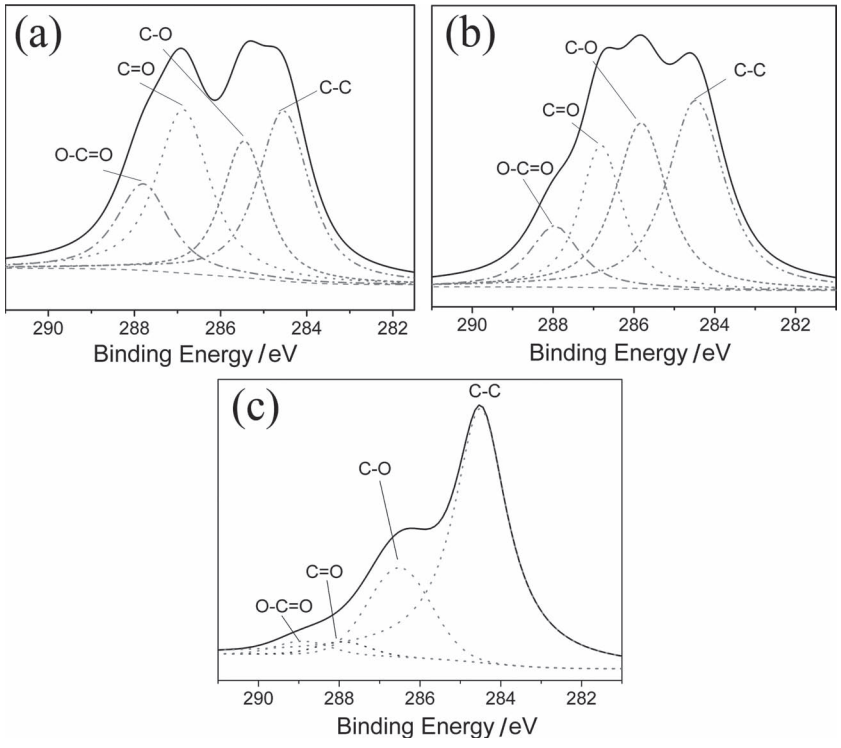


Figure 6. The C1s XPS spectra of GO (a), GNS/$\beta$-CD (b), and GNS only (c) are obtained by means of a RBD upgraded PHI-5000C ESCA system with A1K$\alpha$ radiation ($h\nu$ = 1486.6 eV).

NANO MICRO small

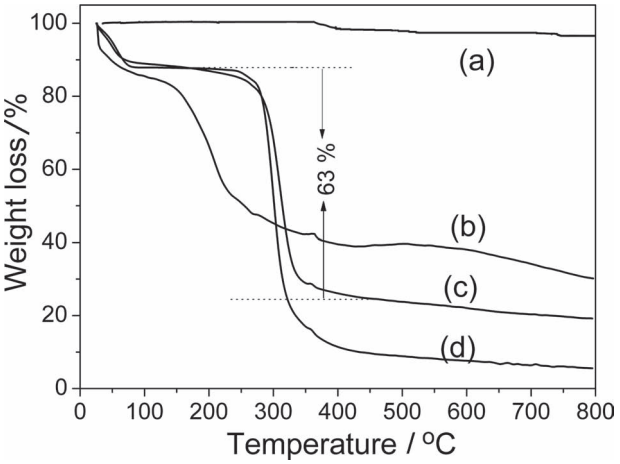


**Figure 7.** TGA curves of flake graphite (a), GO (b), GNS/β-CD hybrid (c), and β-CD (d) obtained under a nitrogen flow of 100 mL $min^{-1}$ with the heating rate of 5 °C $min^{-1}$.

of C–O peak for GNS only (Figure 6c). The above results further indicate successful reduction of GO.

The content of β-CD in GNS/β-CD hybrid was determined by thermogravimetric analysis (TGA). The component of flake graphite, GO, as well as β-CD as the control, were also analyzed. As is well known, GO is thermally unstable with steps of mass loss at elevated temperatures. As shown in **Figure 7**b, there is a slight weight loss below 100 °C, due to evaporation of water, and about 45% mass loss around 180~400 °C, presumably attributed to the pyrolysis of the thermally-labile, oxygen-containing functional groups.[34] The mass loss above 400 °C is attributed to the bulk pyrolysis of carbon skeleton, which is similar to graphite Figure 7a. In contrast, the removal of the thermally labile oxygen functional groups via chemical reduction enhances the thermal stability of graphene nanosheet. As shown in Figure 7c, only insignificant mass loss was observed around 200 °C due to the small quantity of residual oxygen-containing groups, suggesting the removal of most of the oxygen-containing functional groups. The pronounced mass loss in the range from 250 °C to 350 °C is linked to thermal decomposition of β-CD, which is consistent with pure β-CD (Figure 7d). The amount of β-CD is determined to be 63% (about one CD per 55 carbon atoms), indicating that a large amount of CD molecules has been anchored on GNS. As shown in **Figure 8**c, the average thickness of GO is 0.876 nm, which is on the order of two layers of graphene, and the lateral size is around 80 nm. In contrast, the average thickness of GNS/β-CD (Figure 8d) is 11.42 nm, much thicker than that of GO, suggesting abundant β-CD anchored on the surface of GNS. Aggregation of GNS is possible before β-CD attachment to afford GNS/β-CD.

### 2.2. Stability, Cytotoxicity, and Hemolysis Assay of the GNS/β-CD Hybrid

For biomedical applications, good dispersion in a physiological medium is a prerequisite. These studies were completed on the colloidal stabilities of GO and GNS/β-CD hybrid in

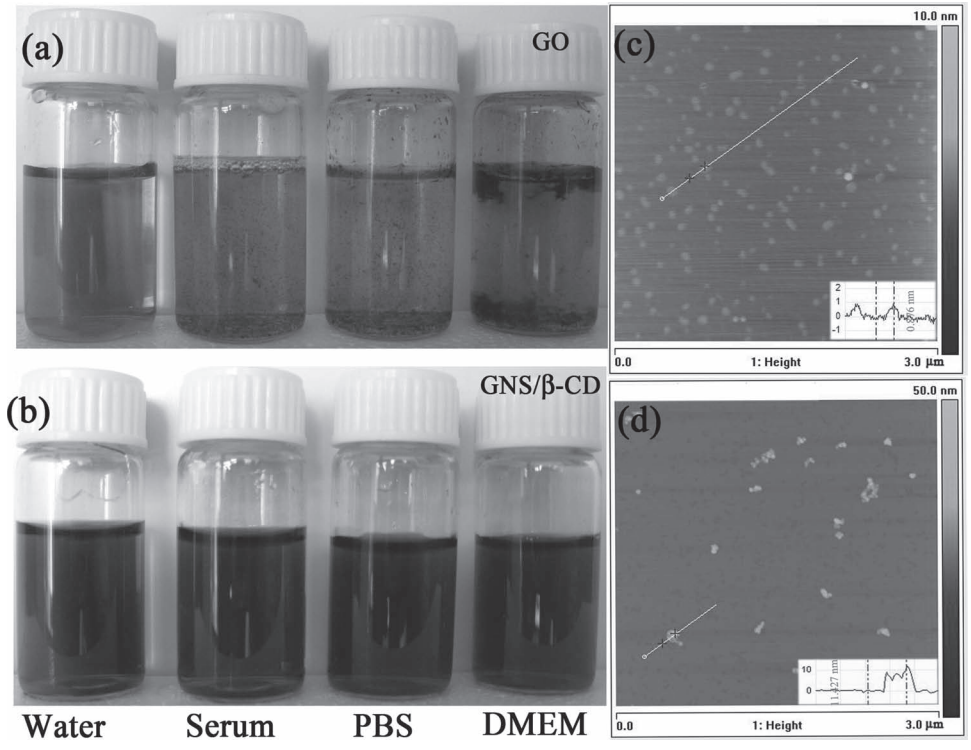


**Figure 8.** Photos of GO (a), GNS/β-CD (b) in different medium and atomic force microscope (AFM) images of GO (c) and GNS/β-CD obtained in tapping mode (d).

different media including water, phosphate buffered saline (PBS), serum and Dulbecco's modified Eagle's medium (DMEM). GO is steadily dispersed in water but aggregated in aqueous solutions that are rich in salts or proteins, such as serum and DMEM (Figure 8). This is probably due to screening of the electrostatic charges and non-specific binding of proteins on GO.[35] In contrast, GNS/β-CD hybrid exhibits excellent stability in all biological solutions for more than one month, showing its great potential in biomedical applications.

Cytotoxicity of GNS/β-CD hybrid was investigated in vitro. HeLa cells were chosen as model cell lines. The experimental results of WST assay show low potent cancer cell killing for GNS/β-CD in vitro with HeLa cells. The cell viability is more than 80% even at a high concentration of 200 mg $L^{-1}$, indicating low cytotoxicity of GNS/β-CD.

In vitro hemolysis assay of healthy human red blood corpuscles was also carried out. **Figure 9** shows optical microscopy analysis of erythrocyte morphology after incubation with pure PBS and GNS/β-CD suspension of different concentrations (10 and 40 mg $L^{-1}$). It is found that nearly all the erythrocyte membranes are kept integrated when incubated with PBS for up to 4 h (Figure 9a,b). Even with erythrocyte surface attached GNS/β-CD, the suspension shows little effect on the erythrocyte morphology and membrane integrity at the dosage of 10 and 40 mg $L^{-1}$ for 1 h (Figure 9c,e). However, erythrocyte membranes experience partial rupture when exposed to 10 and 40 mg $L^{-1}$ for 4 h (Figure 9d,f). In line with this, surface membrane of erythrocytes is progressively compromised by GNS/β-CD in a dose (5, 10, 40 mg $L^{-1}$)-dependent manner. This behavior has lead to the release of free hemoglobin in the medium as evidenced from the UV absorption intensity of hemoglobin at 541 nm. The hemolysis percentages of GNS/β-CD are respectively 20%, 32%, and 49% for the dosage of 5, 10, and 40 mg $L^{-1}$ GNS/β-CD for 4 h. Compared with percent hemolysis of GNS reported (<10% at 40 mg $L^{-1}$ dose for 3 h),[36] the presence of β-CD is the main cause leading to hemolysis.[37] Other factors such as nanomaterials size, incubation time with erythrocytes, and surface charge[36] should also be taken into consideration.

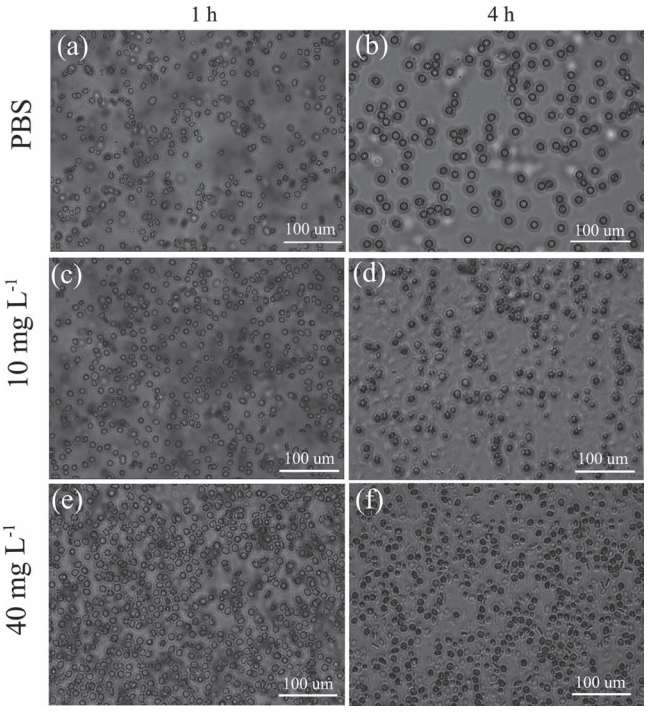


**Figure 9.** Effects of GNS/β-CD concentration and incubation time on morphological changes of human erythrocytes. Exposures to PBS for 1 h (a) and 4 h (b); exposures to GNS/β-CD suspension 10 mg $L^{-1}$ for 1 h (c) and 4 h (d); exposures to GNS/β-CD suspension 40 mg $L^{-1}$ for 1 h (e) and 4 h (f).

### 2.3. Drug Loading Capacity

The payload capacity of GNS/β-CD was investigated. 5,6-carboxyfluorescein (5,6-FAM) was used as a model cargo for its fluorescence and potent interaction with GNS via π–π stacking. The aqueous solution color change was observed from yellow (for FAM only) to dark green (for FAM loaded GNS/β-CD dialysis solution; **Figure 10**b inset). The loading process resulted in a fluorescence quenching of FAM (Figure 10a) due to a photo-induced electron-transfer effect.[22] The loading capacity was studied for GNS with various concentrations of 5,6-FAM. The loading capacity gradually improved at higher concentrations. As shown in Figure 10b, the drug loading ratio can be as high as 110% at the concentration of 0.45 mg $mL^{-1}$. The π–π stacking between 5,6-FAM and GNS is believed to be the major driving force for absorption. Comparing with 178% loading ratio of GO for FAM at the same concentration, the lower drug loading ratio of GNS/β-CD is likely attributed to the reduced surface area resulting from the thicker GNS/β-CD sheets.

CDs are an ideal candidate for developing nanosystem platform with multiple anchoring sites. Their cone shaped cavity can act as hosts for a wide variety of functional and biological guest molecules to form host–guest inclusion complexes, driven by geometric compatibility and hydrophobic interactions. Ad-$NH_2$, an anti-virus drug, was chosen as a model

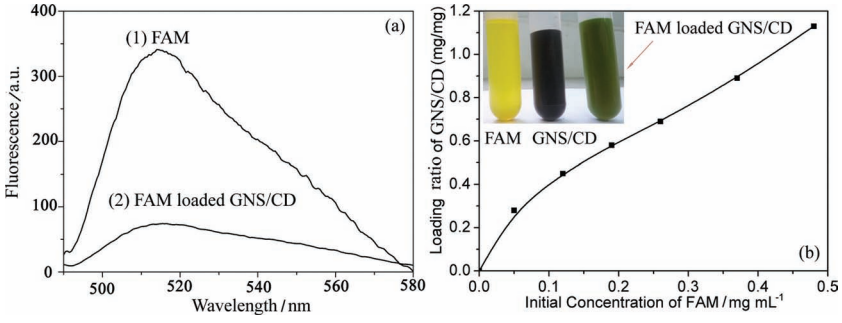


**Figure 10.** (a) Fluorescence spectra of FAM and FAM loaded GNS/CD in water at 492 nm excitation wavelength. Significant fluorescence quenching is observed for FAM loaded GNS/CD. (b) The loading ratio of 5,6-FAM on GNS/β-CD at different concentrations. Inset is the photos for FAM, GNS/β-CD and FAM loaded GNS/β-CD aqueous solution.

NANO MICRO small

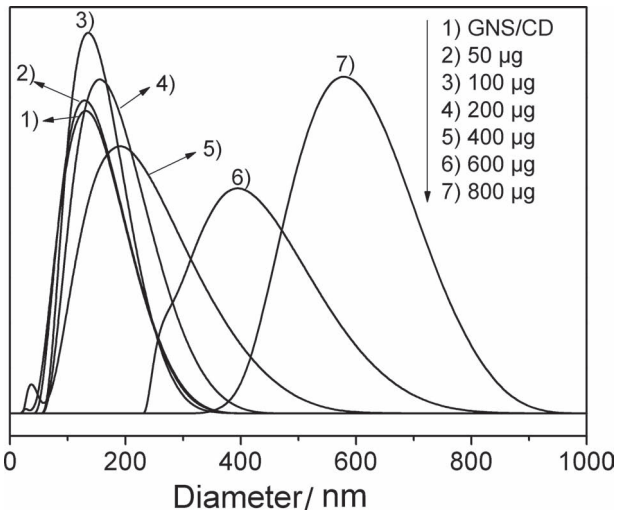


**Figure 11.** Size change of GNS/β-CD (0.2 mg mL$^{-1}$) upon addition of different amounts of Ad-$NH_2$.

drug to investigate the loading capability of GNS/β-CD hybrid *via* host–guest interaction. The storage of Ad-$NH_2$ within the hybrid was confirmed by size change of GNS/β-CD upon addition of Ad-$NH_2$. As shown in **Figure 11**, the size of GNS/β-CD gradually increases by adding Ad-$NH_2$. This behavior is associated with the inclusion of Ad-$NH_2$ in the β-CD cone.

$^1$H NMR experiment was employed to further investigate the inclusion complex of Ad-$NH_2$ and β-CD, as the proton environments of both host and guest usually change upon binding. The internal H-3 and H-5 protons in β-CD are more sensitive to complexation than those outside the host cavity (H-1, H-2, and H-4).[26] As shown in Figure 4, an upfield shift of H-5 signals of β-CD and the downfield shift for characteristic signals of Ad-$NH_2$ locating at approx. 2 ppm are observed after the loading process. The peak shape change is also observed for Ad-$NH_2$ in the range of 0.8–1.2 ppm, as shown in Figure 4c,d. In addition, the intensified signals for Ad-$NH_2$ are detected with the increased dosage of Ad-$NH_2$, as described in the experimental section. The weight loading ratio of Ad-$NH_2$ is calculated to be 3.88% and 5.71%, respectively, which are close to the Ad-$NH_2$ feed ratio (4.0 wt%, 6.67 wt%).

### 2.4. Cell Targeting Study

For active targeting effect using the "host–guest" strategy, cyclic RGD conjugated Ad (Ad-RGD) was used as the targeting moiety and surface-functionalized onto the GNS/β-CD hybrid. The cyclic RGD peptide selectively recognizes $\alpha_v\beta_3$ and $\alpha_v\beta_5$ integrin receptors, which plays a pivotal role in angiogenesis, vascular intima thickening, and proliferation of malignant tumors.[38] HeLa cells possessing $\alpha_v\beta_3$ and $\alpha_v\beta_5$ integrins were chosen as model cell lines to investigate the targeting effect. The endocytosis experiments with and without RGD shielding was completed in order to investigate the targeting effect of Ad-RGD loaded GNS/β-CD (GNS/β-CD/Ad-RGD) on HeLa cells. Since the fluorescence of GNS is barely detectable, FAM was loaded onto GNS/β-CD for fluorescence signal detection. From the images of confocal laser scanning microscopy (CLSM) shown in **Figure 12**, there is a sharp contrast in fluorescent signals between GNS/β-CD/Ad-RGD (strong) and GNS/β-CD (weak). The green signals are the weakest in cells pre-incubated with free RGD-Ad followed by further incubation with FAM-loaded GNS/β-CD/Ad-RGD. These experimental results indicate the interactions between the free RGD-Ad and the integrin receptors. However, interactions of receptors with RGD-Ad loaded FAM/GNS/β-CD are strongly hampered, leading to a lower uptake of FAM-loaded GNS/β-CD/Ad-RGD via integrin-mediated endocytosis. Consistent with the results of flow cytometric analysis (FCA), there is significant FAM fluorescence difference between HeLa cells treated with FAM-loaded GNS/β-CD/Ad-RGD and the control experiments. This is a clear evidence of strong targeting effect due to RGD-Ad loaded GNS/β-CD (**Figure 13**).

Importantly, several other different functional moieties can also be loaded onto this carrier system. For example, the anticancer drug Dox-Ad and polyarginine-Ad with transmembrane capability can be easily loaded onto the template at the same time. Furthermore, our previous work has shown the controlled release of bio-agents, which is regulated by adding competitive guest molecules, *via* the reversibility of host–guest interaction.[26]

## 3. Conclusion

In summary, a unique GNS/β-CD system has been developed from exfoliated GO and β-cyclodextrin. The versatile system

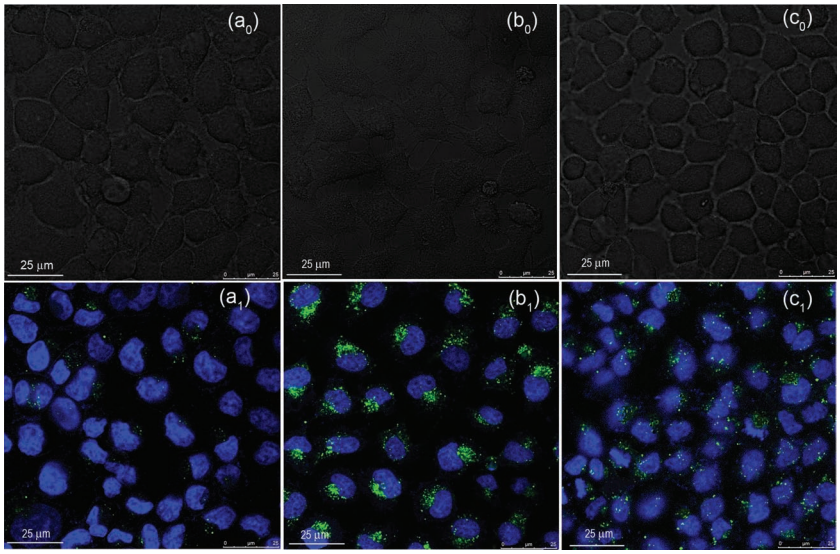


**Figure 12.** Representative confocal laser scanning micrographs of cellular uptake of FAM loaded GNS/β-CD/Ad-RGD for HeLa cells preincubation with ($a_1$) or without ($b_1$) RGD-AD for 2 h followed by another 8 h incubation, ($c_1$) cellular uptake of FAM loaded GNS/β-CD (excitation wavelength: 488 nm).

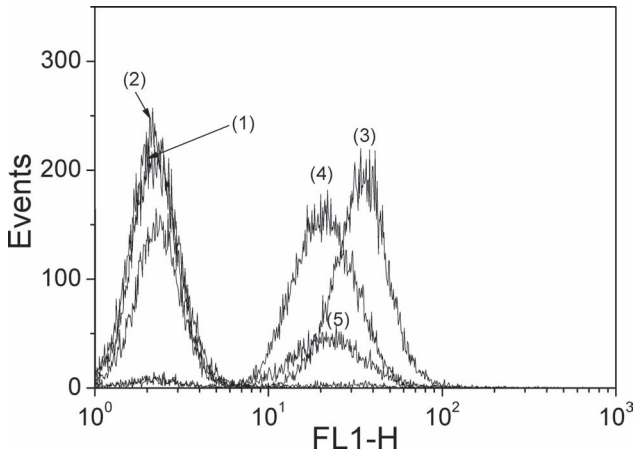


**Figure 13.** Flow cytometric analysis of HeLa cells nontreated (1) and treated by GNS/β-CD (2), FAM loaded GNS/β-CD/Ad-RGD (3), FAM loaded GNS/β-CD (4) and free Ad-RGD pretreated HeLa cells incubated with GNS/β-CD/Ad-RGD (5).

combines the advantages of graphene and cyclodextrins that provide multifunctional and inter-reversible anchor sites. The hybrid is found to possess a high drug-loading capacity and strong targeting effect. These functionalities are easily assembled, in a reproducible and controlled fashion. The hybrid can serve as a basic unit for the assembling of a variety of complex system depending upon the specific biomedical requirements. The model hybrid tested in this investigation has demonstrated a high drug loading efficiency and strong cell targeting capability.

## 4. Experimental Section

*Chemicals*: Flake graphite was purchased from Shanghai Yifan Graphite Co., Ltd., with an average particle diameter of 25 μm (purity > 99.9%). $H_2SO_4$ (AR, 98%), $H_2O_2$ (AR, 30%), $NaNO_3$ (AR), $KmnO_4$ (AR), and $NH_3{\cdot}H_2O$ (25%) were obtained from Sinopharm Chemical Reagent Co. Ltd. The drug model 5(6)-carboxyfluorescein (5(6)-FAM) and β-cyclodextrin (β-CD) were purchased from Aladdin Chemistry. Co. Ltd. Amantadine (Ad-$NH_2$) was obtained from Ad-$NH_2$·HCl by removing HCl under alkaline solution followed by repeated precipitation and extraction process. c(RGDfk)-Ad was purchased from GL Biochem, Ltd. (Shanghai).

*Characterization*: Fourier transform infrared (FTIR) spectra were collected using a Tensor 27 FTIR spectrometer (Bruker AXS, China). UV-vis spectra were recorded on an UV-vis spectrophotometer (Varian, Ltd, Hong Kong) with a sample concentration of 0.05 mg $mL^{-1}$. $^1$H-Nuclear magnetic resonance ($^1$H NMR) spectra were acquired using the Avance III 400 MHz spectrometer (Bruker), DMSO-*d*6 was used as solvent. X-ray diffraction (XRD) were carried out on a D/max2550VB3+/PC X-ray diffractometer (Rigaku International Corporation, Japan) using CuKα radiation (40 kV, 100 mA) with a scanning rate of 4° $min^{-1}$ at 20 °C. Raman spectra were collected from 800 $cm^{-1}$ to 2000 $cm^{-1}$ on a Raman spectrometer (Renishaw inVia Reflex, UK) with argon ion laser emitting at 514.5 nm (20 mW). Atomic force microscope (AFM) images were obtained using a Veeco Dimension 3100 atomic force microscope in the tapping mode for the morphological analyses. Thermogravimetric analysis (TGA) was performed on a STA 449C Jupiter (Netzsch, Germany) under a nitrogen flow of 100 mL $min^{-1}$. All samples were heated from room temperature to 800 °C at a heating rate of 5 °C $min^{-1}$. X-ray photoelectron spectroscopy (XPS) was carried out by means of a RBD upgraded PHI-5000C ESCA system (RBD Enterprises, USA) with A1Kα radiation ($h\nu$ = 1486.6 eV). The size distribution of GNS/β-CD was determined by Zeta Sizer Nano ZS (ZEN 3690, Malvern). The cellular uptake was observed using fluorescence microscopy (Nikon ECLIPSE 80i) and Laser Scanning Confocal Microscope (Leica TCS SP5 II, Germany). Flow cytometric analysis was carried out by FACS Calibur Flow Cytometer (BD Biosciences, USA).

*Preparation of GO*: Graphene oxide was synthesized according to the modified Hummers' method from flake graphite.[39] The size of GO was controlled by adjusting additional amount of oxidation agent and oxidation time.[14]

*Preparation of GNS/β-CD Nanohybrid*: In a typical process for reduction of GO to GNS, β-cyclodextrin (40 mg) were added into homogeneous graphene oxide aqueous suspension (25 mL 0.1 mg $mL^{-1}$), followed by vigorous stirring for 0.5 h under ultrasonication (100 W, 40 KHz). Ammonia solution (25% w/w, 20 μL) was subsequently added into the mixture. After being vigorously stirred for a few minutes, the mixture was allowed to react for 2 h at 80 °C. The mixture was cooled to room temperature and dialyzed against the deionized water to remove the superfluous β-CD and ammonia solution. Finally, a black stably dispersed graphene aqueous dispersion was obtained. Partial was sampled and freeze-dried for the following characterizations.

*Preparation of the Inclusion Complex of GNS/β-CD with Ad-$NH_2$ or Ad-RGD*: The inclusion complexation of β-CD on GNS/β-CD with its matched guest molecule Ad-$NH_2$ was carried out by mixing the GNS/β-CD (0.2 mg $mL^{-1}$, 30 mL) with different dosage of Ad-$NH_2$ (2 mg $mL^{-1}$, 120 μL and 200 μL respectively) in aqueous solution. After shaking for several hours, the mixture was dialysis against water exhaustedly followed by freeze-drying and characterized by $^1$H NMR. The weight loading ratio of Ad-$NH_2$ was calculated by combination of $^1$H NMR and TGA data of GNS/β-CD. The molar ratio of β-CD and Ad-$NH_2$ can be obtained from the ratio of the integrated area of the characteristic peak (H-1) of β-CD and the peak at 1.50~2.01 ppm for Ad-$NH_2$. The inclusion complex behavior was also monitored by DLS. The size change of GNS/β-CD was observed upon addition of Ad-$NH_2$. Ad-$NH_2$ was added, with gradually increasing amount, into GNS/β-CD aqueous solution (0.2 mg $mL^{-1}$, 1 mL) in a cell. The size change was real-time monitored. The inclusion complex of β-CD on GNS/β-CD with Ad-RGD was carried out according above procedure; Ad-RGD (200 μg) was added to GNS/β-CD aqueous solution (0.2 mg $mL^{-1}$, 4 mL). The GNS/β-CD/Ad-RGD hybrid was obtained by dialysis against the mixture against water, followed by centrifugation.

*Loading of 5,6-FAM onto GNS/β-CD or GNS/β-CD-Ad-RGD Nanohybrid*: The loading of 5,6-FAM was carried out by simply mixing GNS/β-CD or GNS/β-CD-Ad-RGD with the given amount of 5,6-FAM. The loading of FAM onto GO was also carried out as a control following the same loading protocol of that GNS/β-CD. In detail, GNS/β-CD aqueous solution (0.05 mg $mL^{-1}$, 10 mL) was first sonicated with a given concentration of 5,6-FAM for 0.5 h, and then stirred for 12 h at room temperature in the dark. The mixture was then ultracentrifuged at 13000 rpm for 1 h and the supernatant was collected. The UV spectrum of the supernatant was

  

NANO MICRO small

measured at 492 nm and the amount of the unloaded 5,6-FAM was estimated according to the standard curve of 5,6-FAM. Consequently, the amount of 5,6-FAM loaded onto the hybrid was calculated by excluding the unloaded part in supernatant from the initial dose. The drug loading ratio was calculated from the following formula:

$$\text{Drug loading ratio (\%)} = (\text{weight of loaded drug/weight of nanohybrid}) \times 100\%$$

*Cell Lines*: The human epitheloid cervix carcinoma (HeLa) cells were supplied by Cell Center of Tumor Hospital of Fudan University (Shanghai, China). Cells were propagated in T-75 flasks under an atmo-sphere of 5% $CO_2$ at 37 °C and grown in DMEM supplemented with fetal bovine serum (10%) and penicillin–streptomycin (0.1%).

*In vitro Cytotoxicity of GNS/β-CD by WST-1 Assay*: Cytotoxicity of GNS/β-CD against HeLa cells was determined by standard WST-1 assay using WST-1 cell proliferation and cytotoxicity assay kit. In brief, HeLa cells were seeded in 96-well plates (5000 cells $well^{-1}$) using DMEM medium (200 μL), and incubated at 37 °C for 24 h. The medium in each well was then replaced with culture medium containing GNS/β-CD (150 μL). The concentration of GNS/β-CD was diluted with culture medium to obtain a concentration range from 0 to 263 mg $L^{-1}$. After incubation for 24 h, the medium in each well was replaced with fresh medium (100 μL) and WST-1 solution (10 μL). The plate was incubated for another 4 h at 37 °C, allowing viable cells to reduce WST-1 into the orange formazan. The plate was read at 450 nm on a Bio-Rad microplate reader (Thermo Fisher Scientific, Waltham, MA, USA).

The relative cell viability (%) was calculated by the following equation: Cell viability = $(OD_{treated}/OD_{control}) \times 100\%$, where $OD_{treated}$ was obtained in the presence of GNS/β-CD and $OD_{control}$ was obtained from the incubation medium. Data are presented as average±SD (n = 6).

*Cellular Uptake of GNS/β-CD/FAM and Targeting Performance:* To monitor cellular uptake of GNS/β-CD/FAM as well as the targeting effect of RGD loaded GNS/β-CD/FAM, HeLa cells ($1 \times 10^5$ cells $well^{-1}$) were incubated with exposure to several different groups: i.e. GNS/β-CD/FAM, and GNS/β-CD/Ad-RGD/FAM pre-incubated initially with or without free Ad-RGD for 2 h, respectively. After incubation at 37 °C for 8 h, the culture medium was removed and cells were rinsed three times with DPBS. Then paraformaldehyde (4%) was added and kept at room temperature for 15 min. The cells were rinsed twice again with DPBS, and imaged by laser scanning confocal microscope (Leica TCS SP5 II, Germany).

Cellular uptake of above three types of materials was also measured by flow cytometric analysis (FACS). Briefly, HeLa cells were seeded in 6-well plate at $1 \times 10^5$ cells $well^{-1}$ and incubated for 24 h. The cells were then incubated at 37 °C with GNS/β-CD, GNS/β-CD/FAM, and GNS/β-CD/Ad-RGD/FAM pre-incubated initially with or without free Ad-RGD for 2 h, respectively. After incubation for 8 h, cells were washed with DPBS twice and harvested, then suspended in paraformaldehyde (2%, 500 μL) for FACS analyses using FACS Calibur flow cytometer (BD Biosciences, USA).

*Observation of the Erythrocyte Morphology and Erythrocyte Hemolysis Assay*: In vitro hemolysis assay was carried out as described.[36] Briefly, fresh EDTA-stabilized human whole blood sample was collected from healthy volunteer. Typically, whole blood (2 mL) was added to PBS (4 mL) and centrifuged at 4000 rpm for 5 min at 4 °C (Thermal Fisher Electron Corporation, Heraeus Biofuge Strators, Germany) to separate erythrocytes. The purification step was repeated four times, and washed erythrocytes were finally re-suspended to the desired hematocrit level using the same buffer and stored at 4 °C and used within 6 h of sample preparation.

The effect of GNS/β-CD on the erythrocyte morphology changes was investigated by optical microscopy. Erythrocyte suspension (10% hematocrit) was incubated with various doses of GNS/β-CD suspension. At different time intervals, 100 μL of these incubated mixtures were dropped onto glass slide and erythrocyte shape changes were observed by optical microscopy directly; the overall magnification was 400×.

The in vitro effect of human erythrocyte hemolysis by GNS/β-CD was evaluated according to the procedures described elsewhere.[40,41] An erythrocyte suspension (10% hematocrit) was exposed to different concentrations of GNS/β-CD in PBS. In order to obtain positive and negative controls, erythrocytes were suspended either in deionized water or PBS, respectively.

Samples were incubated in a rocking shaker at 37 °C for 4 h, a volume of 200 μL of the samples was removed and diluted with PBS (3.8 mL) and centrifuged at 4000 rpm for 10 min. The absorbance of the resulting supernatant (A) as well as the positive and negative controls were measured at 541 nm by a UV-Vis spectrophotometer. Percent hemolysis was calculated using the following equation:

$$\text{Percent hemolysis (\%)} = \frac{\text{Samples Abs 541 nm} - \text{Negative control Abs 541 nm}}{\text{Positive control Abs 541 nm} - \text{Negative control Abs 541 nm}} \times 100\%$$

## Supporting Information

*Supporting Information is available from the Wiley Online Library or from the author.*

## Acknowledgements

*This research is supported by National Natural Science Foundation of China (21104059, 51173136, 51073121), Large Scale Instrument Fund of Tongji university (2011032, 2011033) and "Chen Guang" project supported by Shanghai Municipal Education Commission and Shanghai Education Development Foundation.*

[1] Y. Guo, D. L. Shi, H. S. Cho, Z. Y. Dong, A. Kulkarni, G. M. Pauletti, W. Wang, J. Lian, W. Liu, L. Ren, Q. Q. Zhang, G. K. Liu, C. Huth, L. M. Wang, R. C. Ewing, *Adv. Funct. Mater.* **2008**, *18*, 2489.
[2] D. L. Shi, N. M. Bedford, H. S. Cho, *Small* **2011**, *7*, 2549.
[3] Y. Y. Shao, J. Wang, H. Wu, J. Liu, I. A. Aksay, Y. H. Lin, *Electroanal.* **2010**, *22*, 1027.
[4] Y. Wang, Z. Li, J. Wang, J. Li, Y. Lin, *Trends Biotechnol.* **2011**, *29*, 205.
[5] L. Feng, Z. Liu, *Nanomedicine* **2011**, *6*, 317.
[6] L. M. Zhang, J. G. Xia, Q. H. Zhao, L. W. Liu, Z. J. Zhang, *Small* **2010**, *6*, 537.

  

[7] X. Y. Yang, X. Y. Zhang, Y. F. Ma, Y. Huang, Y. S. Wang, Y. S. Chen, *J. Mater. Chem.* **2009**, *19*, 2710.
[8] Y. Yang, Y. M. Zhang, Y. Chen, D. Zhao, J. T. Chen, Y. Liu, *Chem. Eur. J.* **2012**, *18*, 4208.
[9] K. J. Huang, D. J. Niu, J. Y. Sun, C. H. Han, Z. W. Wu, Y. L. Li, X. Q. Xiong, *Colloid Surf. B* **2011**, *82*, 543.
[10] X. M. Sun, Z. Liu, K. Welsher, J. T. Robinson, A. Goodwin, S. Zaric, H. J. Dai, *Nano Res.* **2008**, *1*, 203.
[11] X. B. Fan, W. C. Peng, Y. Li, X. Y. Li, S. L. Wang, G. L. Zhang, F. B. Zhang, *Adv. Mater.* **2008**, *20*, 4490.
[12] Y. Si, E. T. Samulski, *Nano Lett.* **2008**, *8*, 1679.
[13] Z. Liu, J. T. Robinson, X. M. Sun, H. J. Dai, *J. Am. Chem. Soc.* **2008**, *130*, 10876.
[14] H. Q. Dong, Z. L. Zhao, H. Y. Wen, Y. Y. Li, F. F. Guo, A. J. Shen, P. Frank, C. Lin, D. L. Shi, *Sci. China Chem.* **2010**, *53*, 2265.
[15] K. Yang, J. M. Wan, S. A. Zhang, Y. J. Zhang, S. T. Lee, Z. A. Liu, *ACS Nano* **2011**, *5*, 516.
[16] H. Q. Hu, J. H. Yu, Y.Y. Li, J. Zhao, H. Q. Dong, *J. Biomed. Mater. Res. A* **2011**, *100A*, 141.
[17] V. K. Rana, M. C. Choi, J. Y. Kong, G. Y. Kim, M. J. Kim, S. H. Kim, S. Mishra, R. P. Singh, C. S. Ha, *Macromol. Mater. Eng.* **2011**, *296*, 131.
[18] S. Zhang, K. Yang, L. Feng, Z. Liu, *Carbon* **2011**, *49*, 4040.
[19] Y. Guo, S. Guo, J. Ren, Y. Zhai, S. Dong, E. Wang, *ACS Nano* **2010**, *4*, 4001.
[20] J. Gao, F. Liu, Y. Liu, N. Ma, Z. Wang, X. Zhang, *Chem. Mater.* **2010**, *22*, 2213.
[21] K. P. Liu, J. J. Zhang, F. F. Cheng, T. T. Zheng, C. M. Wang, J. J. Zhu, *J. Mater. Chem.* **2011**, *21*, 12034.
[22] H. Y. Wen, C. Y. Dong, H. Q. Dong, A. J. Shen, W. J. Xia, X. J. Cai, Y. Y. Song, X. Q. Li, Y. Y. Li, D. Shi, *Small* **2012**, *8*, 760.
[23] M. V. Rekharsky, Y. Inoue, *Chem. Rev.* **1998**, *98*, **1875**.
[24] A. Harada, A. Hashidzume, Y. Takashima, *Adv. Polym. Sci.* **2006**, *201*, 1.
[25] H. Q. Dong, Y. Y. Li, L. Li, D. L. Shi, *Prog. Chem.* **2011**, *23*, 914.
[26] H. Q. Dong, Y. Y. Li, H. Y. Wen, M. Xu, L. J. Liu, Z. Q. Li, F. F. Guo, D. Shi, *Macromol. Rapid Commun.* **2011**, *32*, 540.
[27] C. Z. Zhu, S. J. Guo, Y. X. Fang, S. J. Dong, *ACS Nano* **2010**, *4*, 2429.
[28] A. C. Ferrari, J. Robertson, *Phys. Rev. B* **2000**, *61*, 14095.
[29] S. Stankovich, D. A. Dikin, R. D. Piner, K. A. Kohlhaas, A. Kleinhammes, Y. Jia, Y. Wu, S. T. Nguyen, R. S. Ruoff, *Carbon* **2007**, *45*, 1558.
[30] V. López, R. S. Sundaram, C. Gómez-Navarro, D. Olea, M. Burghard, J. Gómez-Herrero, F. Zamora, K. Kern, *Adv. Mater.* **2009**, *21*, 4683.
[31] D. R. Dreyer, H. P. Jia, C. W. Bielawski, *Angew. Chem.* **2010**, *122*, 6965.
[32] D. R. Dreyer, S. Murali, Y. Zhu, R. S. Ruoff, C. W. Bielawski, *J. Mater. Chem.* **2011**, *21*, 3443.
[33] A. Buchsteiner, A. Lerf, J. Pieper, *J. Phys. Chem. B* **2006**, *110*, 22328.
[34] S. Park, J. H. An, R. D. Piner, I. Jung, D. X. Yang, A. Velamakanni, S. T. Nguyen, R. S. Ruoff, *Chem. Mater.* **2008**, *20*, 6592.
[35] N. W. S. Kam, Z. Liu, H. J. Dai, *J. Am.Chem. Soc.* **2005**, *127*, 12492.
[36] K. H. Liao, Y. S. Lin, C. W. Macosko, C. L. Haynes, *ACS Appl. Mater. Inter.* **2011**, *3*, 2607.
[37] Y. Ohtani, T. Irie, K. Uekama, K. Fukenaga, J. Pitha, *Eur. J. Biochem.* **1989**, *186*, 17.
[38] M. Oba, S. Fukushima, N. Kanayama, K. Aoyagi, N. Nishiyama, H. Koyama, K. Kataoka, *Bioconj. Chem.* **2007**, *18*, 1415.
[39] L. Zhang, J. J. Liang, Y. Huang, Y. F. Ma, Y. Wang, Y. S. Chen, *Carbon* **2009**, *47*, 3365.
[40] X. Zhang, J. Yin, C. Peng, W. Hu, Z. Zhu, W. Li, C. Fan, Q. Huang, *Carbon* **2011**, *49*, 986.
[41] S. K. Singh, M. K. Singh, P. P. Kulkarni, V. K. Sonkar, J. J. A. Gracio, D. Dash, *ACS Nano* **2012**, *6*, 2731.

Received: May 8, 2012
Revised: September 18, 2012
Published online: October 9, 2012

  